



Effect of substrate surface finish and particle velocity on fatigue performance of cold spray coated A6061 aluminum alloy

Ahmad Nourian, Sinan Müftü*

Department of Mechanical and Industrial Engineering, Northeastern University, Boston, MA, USA



ARTICLE INFO

Keywords:

Cold spray
Particle velocity
Substrate surface roughness
Bond strength
Fatigue strength

ABSTRACT

Cold spray coatings made with powder of the same material as the substrate can be used to improve fatigue performance and/or to repair damaged parts. The effects of substrate surface finish and particle impact velocity on the bond strength and fatigue performance of Al-6061-T6 substrates coated with Al-6061 powder by using high pressure cold spray (CS) were investigated. To evaluate the effect of particle velocity, coatings were prepared by using both nitrogen (N_2) and helium (He) as carrier gases. A new method for substrate surface preparation was introduced by low angle spraying (LAS) with the same powder prior to coating. The bond bar specimens in polished, semi-polished, grit-blasted (GB) and low angle sprayed (LAS) conditions were coated and tested for bonding strength. The microstructural characteristics and microhardness profiles of the coated samples were also evaluated. Fatigue tests on uncoated and coated samples were conducted under fully-reversed axial loading in load-controlled condition. The failure mechanism was identified by evaluating the fracture surfaces using scanning electron microscopy. The results showed that both bonding strength and fatigue performance of the coated specimens prepared by using He-gas were significantly higher than those prepared by using N_2 . Among the N_2 -sprayed coatings, the bonding strength of on LAS substrates were significantly higher than that of the other surface conditions, and the bonding strength of coatings on GB substrates was superior to that of polished and semi-polished samples. However, the fatigue performance of LAS-coated samples was inferior compared to uncoated samples due to cracks initiating in the coating and propagating into the substrate. The fatigue behavior of GB-coated specimens was similar to the uncoated samples due to delamination of the coating which resulted in stopping the cracks that initiated in the coating.

1. Introduction

Cold gas-dynamic spray, simply known as cold spray (CS), is a progressive, low temperature solid-state coating process which results in lower thermal effects on the processed materials relative to high temperature processes such as thermal spray. This enables cold spray process to be particularly suitable for many different coating applications for metals and polymers [1–3].

In CS process, the powder feedstock (<50 μm) is accelerated to supersonic velocities (300–1200 m/s) using a preheated compressed gas (He, N_2 , or air) expanding in a convergent-divergent de Laval nozzle. Upon impact with the underlying material, powder particles experience severe plastic deformation, resulting in disruption of the thin oxide film along the interface. Therefore, a direct metal-to-metal contact is established, resulting in bonding through both metallurgical and mechanical mechanisms [4,5]. Effective bonding depends on sufficient deformation

rates provided by high impact velocity. Research shows that there is a critical impact velocity below which the sprayed particles rebound off the substrate [6–8]. The material properties of the powder and the substrate, type of the carrier gas, particle temperature, powder size distribution, oxygen content, and nozzle geometry are among the parameters that affect the particle velocity, the quality of the interfacial bonding, and coating porosity [9–11].

Currently, CS process is typically applied for coating industrial components to improve corrosion and wear resistance and to repair damaged regions. Most CS coatings are used for non-load bearing components for which fatigue performance may not be an issue. With the advances in this technology load-bearing applications will become more common and therefore assessment of fatigue behavior of CS coated surfaces will become a necessity. Several factors can influence the fatigue behavior of CS coatings including coating-substrate interface quality, residual stress, material properties of the coating and substrate,

* Corresponding author.

E-mail addresses: A.nourianavval@northeastern.edu (A. Nourian), S.Muftu@northeastern.edu (S. Müftü).

surface conditions including the roughness of the substrate, and stress gradients [12]. Most studies of fatigue performance of CS coated materials involve dissimilar materials with somewhat contradictory results pointing to the complexity of the problem.

Fatigue performance of CS coated materials was first reported by Price et al. [13]. They coated Ti6Al4V with pure Ti to enhance the biocompatibility and corrosion resistance of the substrate. However, they observed that the long-life fatigue strength of the coated specimens was 15 % lower than that of uncoated specimens. This was thought to be due to roughened surface at the interface which acted as stress concentration site, while low residual stress in the coating and substrate could not prevent fatigue crack initiation. Sansoucy et al. [14] also evaluated the effect of Al-Co-Ce cold spray coating on fatigue resistance of AA2024-T3 aluminum alloy. They observed that the fatigue performance of coated specimens under bending was significantly enhanced compared to uncoated specimens. This result was attributed to high adhesion strength of the coating and compressive residual stress within the coating. Fatigue behavior of Al 7075-T6 specimens coated with pure aluminum by using He and N₂ as process gas was also investigated by Barnes et al. [15]. They observed that fatigue lives of samples coated with N₂ are longer than those of He-sprayed samples. They justified this observation by the probable damage induced on the substrates due to higher particle impact velocity when He is used as the process gas.

It has also been reported that the difference between the material properties of coating and substrate has significant effect on cyclic performance of coated specimens. Ghelichi et al. [16] compared the fatigue properties of 5052 aluminum alloy coated with pure-Al and 7075 aluminum alloy. Fatigue strength of samples coated with Al 7075 was enhanced by 30 % compared to uncoated specimens. Samples with pure-Al coating did not show significant improvement in fatigue performance due to delamination of coating during cyclic loading. In another work, the same authors [17] investigated the fatigue performance of Al 5052 alloy coated with gas-atomized (micro-crystalline) and cryomilled (nano-crystalline) Al 7075 powder under bending. The results showed that the fatigue performance of coated specimens in both cases was improved. However, fatigue lives of the specimens coated with gas-atomized powder were longer than those of cryomilled ones. This was attributed to higher porosity resulting from lower deformability of irregularly-shaped cryomilled powder compared to spherically-shaped atomized case.

Dayani et al. [18] showed that the fatigue performance of cast AZ31B magnesium alloy coated with high strength Al 7075 under rotating-bending condition was improved by 26 % compared to uncoated specimens. They observed the fatigue cracks to primarily initiate from the casting defects within the substrate, while only secondary cracks were identified in the coating due to compressive residual stress which contributed to enhance the fatigue performance. The same conclusions were also made by Yang et al. [19] for fatigue properties of Q355B steel coated with pure-Al and 5052 aluminum alloy.

It has been demonstrated that adding hard particles to metal powders improves the coating quality by reducing the porosity and increasing the bond strength of the coating to the substrate. Xiong et al. [20] evaluated the fatigue performance of AZ91D magnesium alloy, coated with Al + Al₂O₃ composites with different volume fractions of alumina under three-point bending loading. They reported that increasing the volume fraction of Al₂O₃ up to 50 % enhances the fatigue strength due to higher yield strength and work hardening of the substrate surface. Jeong et al. [21] evaluated the fatigue performance of A356 cast aluminum coated with pure Al and Al-25%SiC composite under axial loading. They reported a 200 % increase in fatigue strength in Al-SiC coated specimens at room temperature. This was thought to be due to crack arrestment by SiC particles. The plastic deformation in the substrate induced by the peening effect of SiC particles during deposition also contributed to increasing the crack growth resistance.

It has been proposed that the initial surface finish of the substrate has an important effect on the bond strength between the coating and the

substrate. Although in the past years some work has been reported on the effect of substrate surface finish on coating-substrate bonding [22–26], surface preparation conditions for each new material systems require careful evaluation. Some experimental work reported that grit blasting a substrate results in higher deposition efficiency [22,23]. While a number of researchers believe that polishing or grinding the substrate before coating enhance the coating-substrate bonding strength compared with grit-blasted substrates [24–26]. The effect of pre-deposition surface condition on fatigue performance of CS coated specimens has also been investigated. Ziemian et al. [27] evaluated the effect of grit blasting (GB) and shot peening (SP) on AA2024-T351 substrate coated with pure Al. They reported higher bonding strength and fatigue resistance for GB specimens compared to SP specimens, due to the surface damage caused by heavy and large shots. Moridi et al. [28] also examined the effect of conventional shot peening (SP) and severe shot peening (SSP) before and after cold spray coating on rotating bending fatigue performance of 6082 aluminum alloy. They also reported that shot peening of the specimens prior to CS coating enhanced the fatigue strength by 26 %, while performing shot peening after CS coating damaged the coating-substrate interface, resulting in delamination during cyclic loading.

For evaluation of fatigue performance of CS coated materials, most studies have focused on cantilever bending, three-point bending, and rotating-bending. These loading conditions induce stress gradient with the highest stress on the coating, but the stress gradually decreases toward the core material. However, the gradient stress under these types of loads depends on the thickness of coating and specimens such that bending specimens, which are usually thin, have higher stress gradient compared to rotating bending ones [9]. This fact can affect the fatigue crack initiation and propagation. Only a couple of studies have evaluated the fatigue performance of cold spray coated materials under axial loading [21,29,30].

Most studies of fatigue performance of CS coated materials involve dissimilar materials. As indicated above, fatigue in (CS) coated specimens depends on many factors including: bond-strength of the coating-substrate interface; initial hardness and roughness of the substrate surface; and, residual stresses in the substrate and the coating. To investigate fatigue performance of coated surfaces systematically and to reach a fundamental understanding of the behavior of CS coated materials, simple loading tests with same materials should be conducted. To this end, in this work we report results of a study of fatigue performance of 6061-T6 aluminum alloy coated with Al 6061 powder under fully-reversed tension-compression axial loading. Thus, the effects of non-uniform loading and dissimilar materials are eliminated as problem variables. In particular, the effects of using different surface preparations and particle impact conditions by using two different accelerating gases are investigated. Coating characterization including metallography, hardness testing, and fractography are performed and reported.

2. Experimental procedure

2.1. Coating preparation

Gas atomized Al 6061 powder provided by Solvus Global LLC (Worcester, MA, USA) was used to prepare the cold spray coatings on Al 6061-T6 substrate provided by McMaster-Carr (Elmhurst, IL, USA). Morphology of the particles, as well as particle size distribution are illustrated in Fig. 1. The particles are generally spherical with the diameter quantiles of d₁₀ = 29 μm, d₅₀ = 39 μm, and d₉₀ = 51 μm. The particle size distribution was computed from five SEM images using Zen Core V2.6 (Zeiss, Germany) image analysis software based on the equivalent diameter. The chemical composition of both the substrate and the powder were measured using energy-dispersive X-ray (EDX) spectroscopy, as shown in Table 1, indicating that they match the expected composition of the standard alloy [31].

Cold spray deposition was performed by using a Gen III high pressure

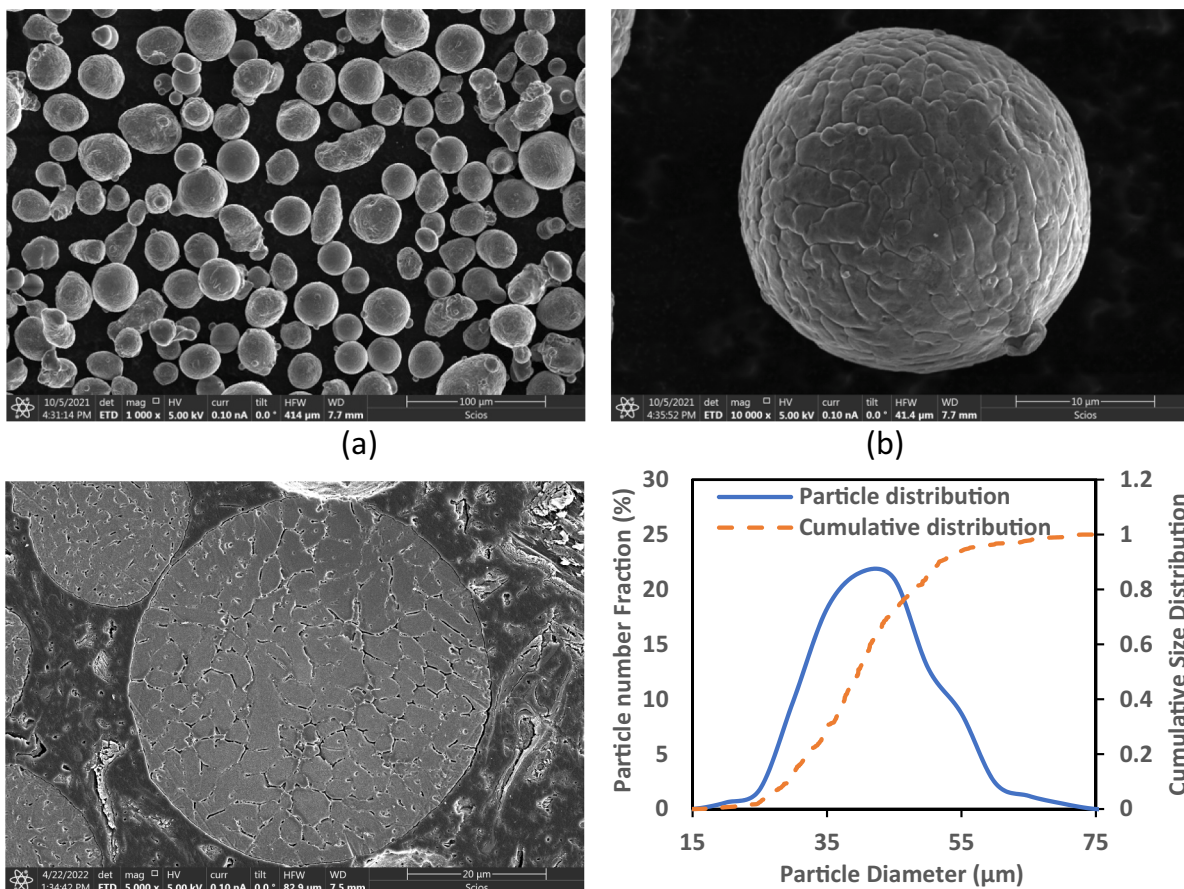


Fig. 1. SEM images showing (a-b) morphology, (c) particle microstructure, and (d) particle size distribution of 6061 powder used in this study. Note that the scale bars in (a), (b) and (c) are 100, 10 and 20 μm , respectively.

Table 1
Chemical composition of the powder and substrate used in this study.

	Mg	Si	Cu	Fe	Mn	Al
Powder	0.84	0.49	0.34	0.10	0.04	Bal.
Substrate	0.91	0.63	0.39	0.07	0.05	Bal.

cold spray system manufactured by VRC Metal Systems (Rapid City, SD, USA). Deposition was performed by using both N_2 and He. He-gas, which has a low molecular weight, can reach higher gas velocities than N_2 , and it is known to provide higher particle impact velocities, higher deposition efficiency and better coating quality. CS process parameters used in this work are provided in **Table 2**. In this work the gas temperature and pressure were limited by the allowable temperature for

Table 2
Cold spray deposition parameters used in this study.

Parameters	Al6061-He	Al6061- N_2
Carrier gas	He	N_2
Gas pressure	40 bar	65 bar
Gas Temperature	425 °C	455 °C
Nozzle Travel Speed	200 mm/s	200 mm/s
Standoff distance	25 mm	25 mm
Step over	0.5 mm	0.5 mm
Spray angle	90°	90°
Nozzle type	PBI	PBI
Nozzle length	170 mm	170 mm
Nozzle throat diameter	1.5 mm	2.0 mm
Nozzle exit diameter	6.0 mm	6.0 mm
Powder feed rate	6.0 rpm	6.0 rpm

the nozzle material and the maximum gas pressure the system can provide, respectively. In the case of N_2 -sprays, gas temperature and pressure were set to their maximum limits in order to achieve fastest gas and particle velocities. In the case of He-sprays, sufficiently high gas velocities were met at the lower pressure level indicated in **Table 2**. A nozzle with smaller throat diameter was used for He-sprays to reduce the gas consumption.

Powder velocities in N_2 and He gas streams at the operating conditions were measured by a laser in-flight diagnosis system (Oseir HiWatch HR, Tampere, Finland), which can diagnose size dependent particle flight velocities, at 25 mm downstream of the nozzle exit plane. The average particle velocities for N_2 and He streams were measured as 752 m/s and 927 m/s respectively, which are about 1.25 and 1.5 times the critical velocity estimated about 600 m/s for this powder [32]. We note that due to the bow shock that develops above a surface when the compressible gas encounters a surface, the particle velocities at impact may be somewhat slower than the measured values [33].

2.2. Bonding strength optimization

Fatigue performance of CS coated materials is affected by the bonding strength of the substrate-to-coating interface. First, a series of tests were conducted to investigate the effects of substrate surface finish to optimize the bonding strength of the N_2 -sprayed samples. Bond bar specimens were prepared by using four different substrate surface finishes including polished (P), semi-polished (SP), grit blasted (GB), and low-angle-spray (LAS) conditions. The LAS condition consisted of spraying the surface with the Al-6061 powder at 30° nozzle orientation to the horizontal surface. He-sprayed bond bar samples were prepared by using the two best performing surface conditions obtained by N_2 -

sprays.

Polished and semi-polished substrates were prepared by using sandpaper with grit size of 1200 and 320, respectively. GB-substrates were blasted by alumina particles with mesh size of 80 ($<175\text{ }\mu\text{m}$) using a manually controlled nozzle. The impact angle was chosen to be approximately 45° to reduce the amount of embedded grits into the substrate. The GB-substrates were then cleaned using ultrasonic vibrator. Six specimens were prepared for each group.

Surface modification can also be achieved by spraying the same spray powder at a low angle. With this approach significant hardening of the substrate surface can be avoided and the risk of embedding non-metallic grit particles into the substrate surface can be reduced. Research shows that the deposition efficiency is reduced at shallow spray angles such that below a critical spray angle no deposition takes place. The critical spray angles for Cu, Ni, and Ti have been reported to be between 40° - 50° [34–36]. In this work as the fourth surface finish, we sprayed Al 6061 powder at 30° (S30) prior to coating as a surface preparation step. The parameters summarized in Table 2 were used for this operation. The surface roughness of the specimens in all surface finish conditions was measured by Mahr Surf V instrument (Mahr, Germany), which are summarized in Table 3.

The bonding strength of the substrate-coating interface was measured via bond bar tests according to ASTM C633 [37]. Coatings were produced on standard cylindrical test samples having 25.4 mm diameter and overall length of 40 mm with different surface finish conditions. The top surface of the coatings was glued to an uncoated sample using FM-1000 adhesive. The assembled parts were then cured at 176°C for 100 min on a fixture that ensures the alignment of the two pieces.

The bonding strength was measured using a 100-kN universal tensile load frame (Shimadzu, Japan) at crosshead speed of 0.02 mm/s. Before testing the coatings, the bonding agent was tested on uncoated specimens. It was observed that the glue fails at an average stress of 68 MPa, which conforms to the product specifications.

2.3. Fatigue sample preparation and coating characterization

Based on the results of the bond strength tests (Section 3.3) GB and S30 were chosen to prepare the surfaces of the dog-bone specimens. Fatigue dog-bone specimens with round cross section were extracted from a 6061-T6 plate according to ASTM E466-21 [38]. The surface roughness of the specimens after machining was measured to be $0.2\text{ }\mu\text{m}$. The specimens were then cleaned and washed with ethanol. One group of specimens was grit-blasted with alumina with particle size of $<175\text{ }\mu\text{m}$ (mesh #80) and cleaned using ultrasonic vibrator prior to CS coating. The second group of specimens was sprayed at 30° using Al 6061 powder and the process parameters summarized in Table 2. Both GB and S30 specimens were then coated by spraying at 90° . Note that the spray angles were measured relative to the substrate surface of the specimen. Different groups of specimens were coated using N_2 and He to

Table 3

Summary of substrate surface roughness and hardness with different surface preparations.

ID	Surface finish	Experimental description	Roughness (μm)	Hardness (HV)
P	Polished	Ground by SiC sand papers up to #1200 grit size	0.15 ± 0.05	112
SP	Semi polished	Ground by #320 SiC sand paper	0.54 ± 0.12	112
GB	Grit blasted	Grit blasted by Al_2O_3 particles (mesh 80)	5.80 ± 0.95	189
S30- N_2	Sprayed at 30°	Sprayed by the Al-6061 particles (using N_2)	1.80 ± 0.31	128
S30- He	Sprayed at 30°	Sprayed by the Al-6061 particles (using He)	2.19 ± 0.35	134

evaluate the effect of particle velocity on fatigue performance. The applied coating thickness in all specimens was 300 μm , which was then ground to 200 μm and polished longitudinally using sandpapers up to grit size of 1200 to reduce the surface roughness of the coatings. The specimen configuration as well as images of coated specimens in as-deposited and polished conditions are shown in Fig. 2.

The coatings were characterized by conducting metallography on cross-section of the specimens. Cold mounting was used to prepare metallography specimens to prevent any microstructural changes during mounting. The specimens were ground with SiC papers up to mesh size of 1200, followed by polishing with diamond suspension of 3 μm scratch size. The final polishing was performed using 0.2 μm SiC suspension. The polished specimens were etched by immersing into Keller's reagent (95 % water, 2.5 % HNO_3 , 1.5 % HCl, 1.0 % HF) for 15 s. The microstructural analysis was conducted using both optical microscopy (Zeiss Axioscope 7, Germany) and scanning electron microscopy (SEM, FEI Scios DualBeam™). Porosity measurement was performed by analyzing optical micrographs of nine random surfaces from three different samples in unetched condition using Zen Core V2.6 image analysis software. Micro Vickers hardness was also conducted from the coating surface into the substrate by Alpha MTH 2000-Z (Pace Technologies, Tucson, AZ, USA) microhardness tester using a maximum force of 0.49 N (50 gf) and a holding time of 20 s.

Axial fatigue tests were performed on coated and uncoated specimens using an Instron servo-hydraulic load frame (Model No. 1350) with a 100 kN load cell. These tests were conducted under load control condition with stress ratio of $R = -1$ and frequency of 10 Hz until failure occurred. Three specimens were tested in each stress amplitude level. The fatigue data were analyzed to obtain the SN diagram for different conditions with a failure probability of 90 % on a semi-log scale based on ASTM E739-10 [39]. Fracture surfaces were then characterized using SEM to evaluate the crack growth mechanism. In addition, the fractured specimens were sectioned, mounted, and polished for optical examination of crack path side profile along the median section.

3. Results and discussion

3.1. Coating microstructure

The optical and SEM micrographs of the coatings prepared using different gases and surface finish conditions (GB and S30) are shown in Figs. 3 and 4, respectively. He-deposited coatings have dense microstructure with strong interparticle bonding where the inter particle interface is not distinguishable. In these coatings, the deposited particles have undergone a significant plastic deformation during deposition, resulting in almost porosity-free coating on both substrate surface finish conditions. Particles in the N_2 -deposited coatings experienced relatively lower level of deformation.

The extent of particle deformation is characterized by the flattening ratio determined from the cross-sectional SEM images. Flattening ratio is the average of the ratio of width of the deposited particles to the initial particle diameter. The diameters of the undeformed particles are estimated by using the conservation of volume between the initial sphere and the final oblate spheroid [40]. Particles with approximate mean diameter of 40 μm were evaluated for both cases. Twenty different particles were evaluated for determining the flattening ratios of each case. The average flattening ratios of the He- and N_2 -sprayed particles were measured to be 1.5 ± 0.09 and 1.2 ± 0.13 , respectively.

Porosity of the coating was evaluated by using the image analyzer software from metallography images. The porosity of the He-sprayed coatings was nearly undetectable (0.017 %), whereas porosity was 0.83 % for the N_2 -sprayed specimens. In the case of grit-blasted substrates, higher porosity can be seen at the coating-substrate interface, resulting in lower interfacial bonding strength, as will be discussed in Section 3.3.

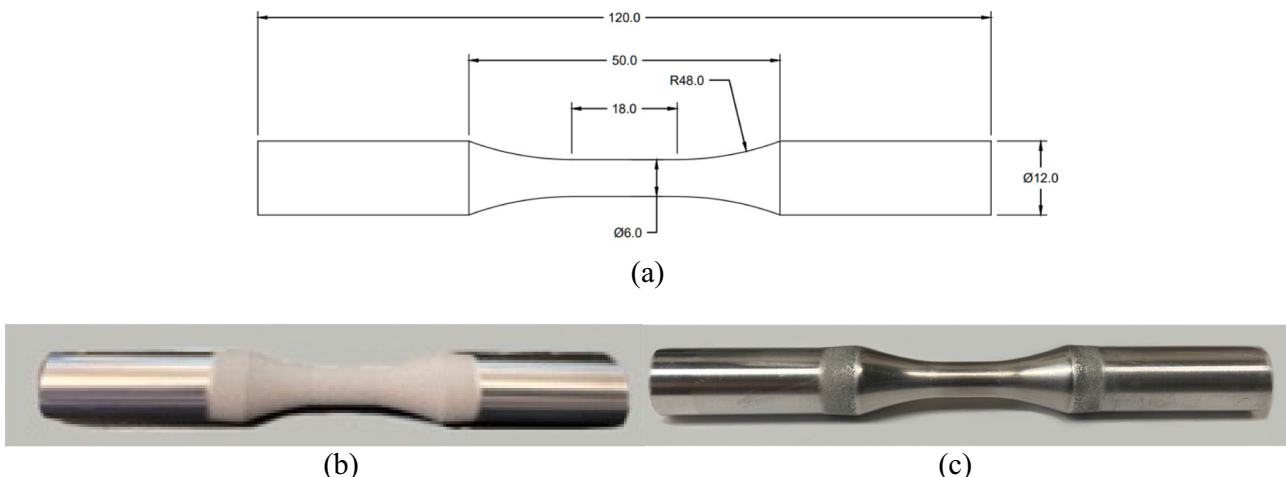


Fig. 2. a) Fatigue specimen configuration used in this study, and images of the coated specimens in (b) as-deposited and (c) polished conditions.

3.2. Microhardness

Variation of microhardness of the coated specimens from the coating surface toward the substrate is illustrated in Fig. 5, whereas Table 3 provides a summary hardness measured from the top of the substrates before coating. The average hardness of the coatings prepared by N₂ and He as accelerating gases was measured as 86.5 ± 7 HV and 105 ± 4 HV, respectively, showing higher hardness of the coatings prepared by He. This is attributed to higher particle impact velocity when He is used as the process gas, resulting in increased plastic deformation and leading to increased hardness in the coatings.

The hardness values for the substrates with different surface preparations are reported in Table 3. After coating, hardness shows a general drop and varies between 105 and 120 HV as shown in Fig. 5. There is a slight dependence on impact velocity where GB-He-coated specimen is harder near the interface. Otherwise, the hardness of the substrate is observed not to be significantly affected by particle impacts. The reduction in hardness is attributed to stress relaxation which may be induced due to high gas temperatures during deposition. Such stress relaxation due to partial annealing during cold spray deposition with high gas temperature has been reported in [15,16,41].

Higher substrate hardness of the GB-He-coated specimens compared to GB-N₂-coated specimens in Fig. 5 may also be due to higher gas temperature for N₂-sprayed specimens compared to He-sprayed cases. Lower flow rate of He gas during deposition, resulting from smaller throat diameter of the used nozzle (see Table 2) could also result in lower temperature on the substrate during deposition, which may affect the hardness of both deposit and the substrate. However, a more detailed study is required for determining the actual reason of this phenomenon.

3.3. Bonding strength

Strength of bonding between the coatings and the substrates with different surface finish, deposited using N₂ or He as accelerating gasses is compared in Fig. 6(a). It was observed that the bonding strength of the coatings deposited using He were above 68 MPa as a result of failure at the glue, while the coatings prepared using N₂ showed lower bond strength and all the coatings failed from the substrate-coating interface. Higher bonding strength of the coatings deposited using He compared to N₂ is due to higher particle velocity which results in stronger metallurgical bonding and mechanical interlocking [42].

Among the specimens coated using N₂ as accelerating gas, the bonding strength of the coating after spraying at 30° is significantly stronger than that of the other surface conditions. The GB-substrates had the second highest bond strength and the coating-substrate bonding

in polished and semi-polished conditions were weak. The fact that the polished surface has a lower bond strength has also been reported by others. Kumar et al. [22] observed that the bonding strength of Cu-on-Cu and Cu-on-Al in polished condition is lower than grit blasted condition. Through finite element analysis, they concluded that frictional dissipation, which is a portion of kinetic energy converted to heat due to friction between the impacting particles and the rough substrate, increases the interface temperature leading to enhanced interfacial bonding compared to polished condition. However, there is a correlation between the substrate surface roughness and hardness, as shown in Fig. 6(b). Increasing the surface roughness results in higher hardness in the substrate due to work hardening which takes place during surface preparation. The work hardening limits the deformability of the substrate during CS deposition and hinders the formation of a primary bonding. Therefore, the lower bond strength of GB-substrates can be attributed to limited deformation of the work-hardened substrate during cold spray deposition. The effect of lower bonding strength resulting from work hardening during grit blasting has also been reported by Tan et al. [43] and Marrocco et al. [25]. They observed that the bonding strength of Ti6Al4V and pure Ti coatings on polished or ground Ti6Al4V substrate is higher than those on grit-blasted substrates. Therefore, it can be inferred that there are two competing factors: increasing the frictional dissipation as a result of surface roughness enhances the bonding strength; and increasing the hardness of the substrate after surface preparation weakens the strength of bonding between the substrate and the coating.

Surface preparation by spraying at 30° results in a slight increase in surface hardness. Therefore, this preparation helps to roughen surface, but still does not impose significant work hardening at the substrate surface. In fact, spraying at low angle is very similar to grit-blasting with very fine blasting media, but in this case the substrate surface is modified without non-metallic particles being embedded into the substrate.

3.4. Fatigue behavior

The SN diagrams obtained with different coating conditions are compared with uncoated specimens in Fig. 7. The stress amplitude in Fig. 7(a) was computed without considering the thickness of the coating, assuming that the coating is not load bearing. While the coating thickness was taken into account for stress computation in Fig. 7(b). As can be seen in Fig. 7(a), N₂-sprayed coatings do not share a significant portion of the applied cyclic loading for both substrate surface finish conditions. Fatigue performance of GB-N₂-coated specimens is similar to that of uncoated specimens, while the S30-N₂-coated specimens have 10 % lower fatigue strength compared to uncoated specimens (see Table 4).

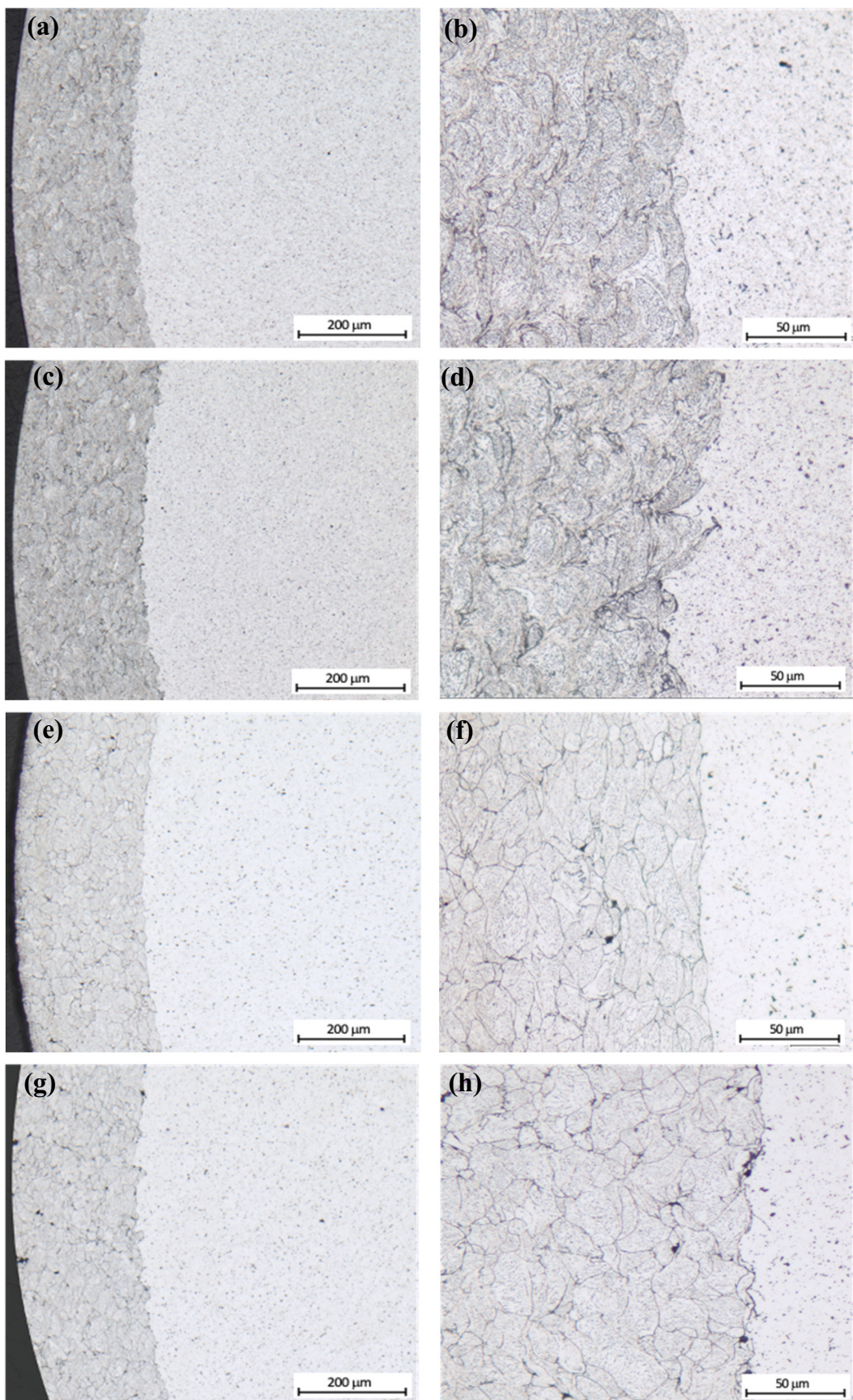


Fig. 3. Optical micrographs of the coated specimens in different conditions; a, b) S30-He-coated, c, d) GB-He-coated, e, f) S30-N₂-coated, and g, h) GB-N₂-coated specimens.

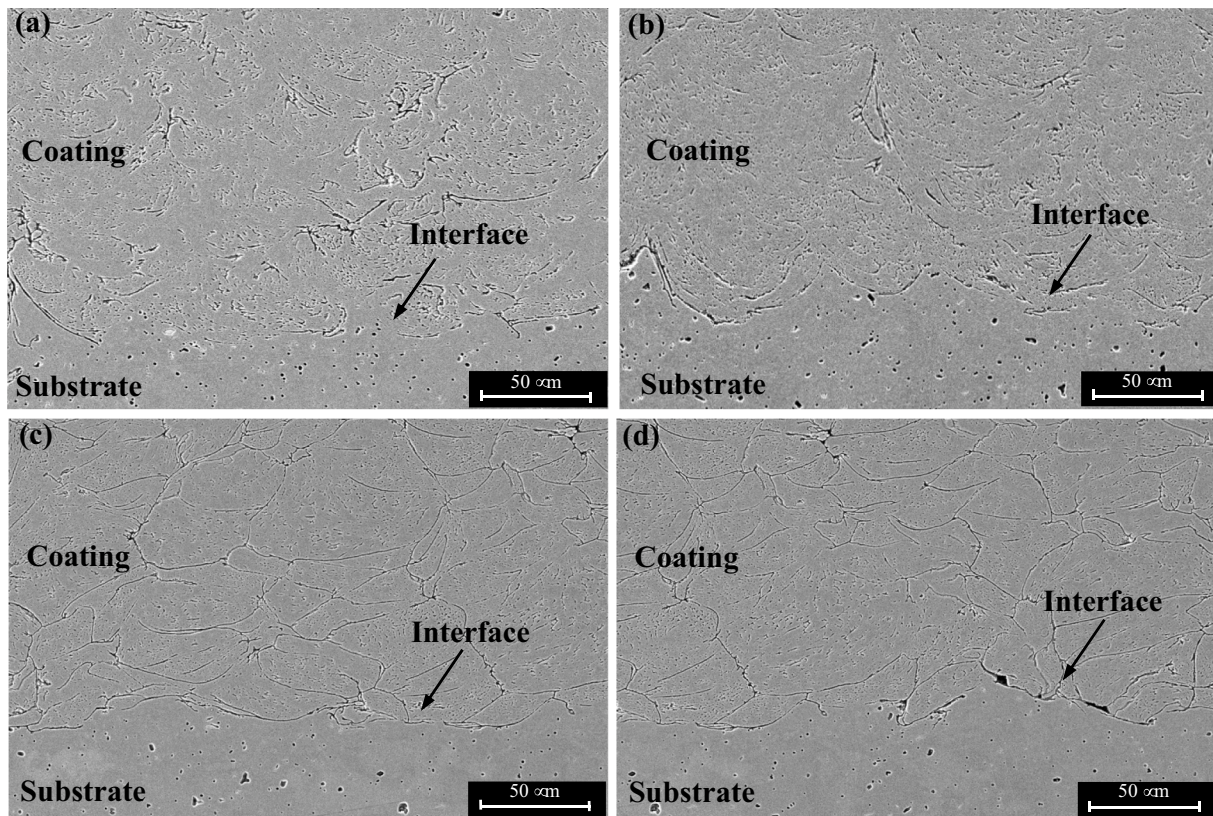


Fig. 4. SEM micrographs of the coated specimens in different conditions; a) S30-He-coated, b) GB-He-coated, c) S30-N₂-coated, and d) GB-N₂-coated specimens.

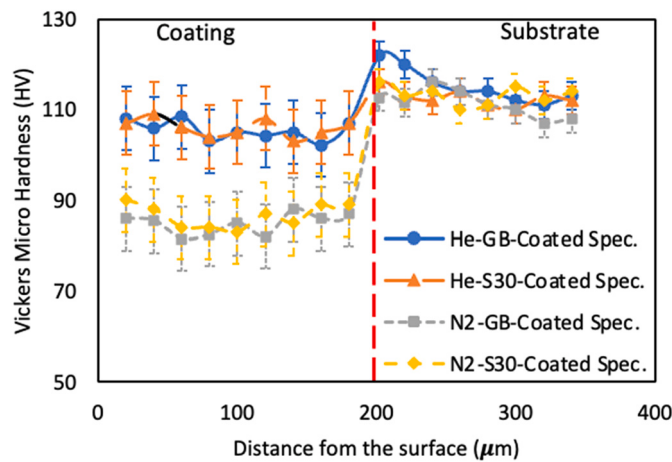


Fig. 5. Microhardness profile from the coating surface toward the substrate.

These findings are in contrast with the bonding strength results, which are significantly higher for the S30-substrates as compared to the GB-substrates.

Coatings deposited with He (at high particle impact velocity) performed like load-bearing materials. Considering the coating as a load bearing material in Fig. 7(b), it can be seen that at high stress levels the fatigue lives of He-sprayed specimens are similar to the uncoated samples, showing that the coating has similar contribution to supporting cyclic loads compared to the substrate material. At lower stress levels, however, the fatigue lives of the He-sprayed samples are longer than those of uncoated samples. Thus, coating specimens with high particle impact velocity, using He gas, results in approximately 20 % improvement in fatigue strength (see Table 4).

The fracture surfaces of the coated specimens presented in Fig. 8 shed light on these observations. As can be seen in this figure, no delamination of the coating can be seen in the S30-N₂-coated specimens during cyclic loading. For the case of the GB-N₂-Coated samples delamination of the coating was observed during fatigue tests. This is due to lower bonding strength of the GB-substrates compared to the S30-N₂-coated ones. Furthermore, initiation of multiple fatigue cracks originating from the pores in the coating or from the unbonded inter-particle regions was observed in fracture surface of the N₂-coated specimens. In the S30-N₂-coated specimens, cracks initiated from the coatings propagated into the substrate, while these cracks could not propagate into the substrate in the GB-N₂-coated specimens as the coating delaminated from the substrate. This result shows that when the bonding strength is sufficiently high to prevent delamination under cyclic loading, the fatigue performance can be affected by CS-characteristic defects such as porosity and unbonded inter-particle regions.

For the specimens coated using He, the coatings were strongly bonded to the substrates and no delamination was observed in both groups of the S30-He-coated and the GB-He-coated specimens. In both cases the fatigue cracks initiated from the unbonded inter-particle regions within the coating and propagated into the substrate.

Fig. 9 shows a high magnification of the fracture surface of the He- and N₂-sprayed specimens. Fig. 9(a) shows that in the N₂-sprayed specimens, fatigue cracks initiated from pores or inter-particle regions/interfaces. In addition, the inter-particle rupture due to weak bonding between the particles as well as beach marks representing fatigue crack propagation can be perceived. Fig. 9(b) shows the crack initiation in the He-sprayed specimens. It can be seen that micro-cracks initiated from the inter-particle regions near the surface. These micro-cracks then coalesced to produce the main crack that propagated and led to final fatigue failure. Therefore, in both cases fatigue cracks initiated from the coating imperfections.

Higher fatigue strength in He-sprayed specimens compared to

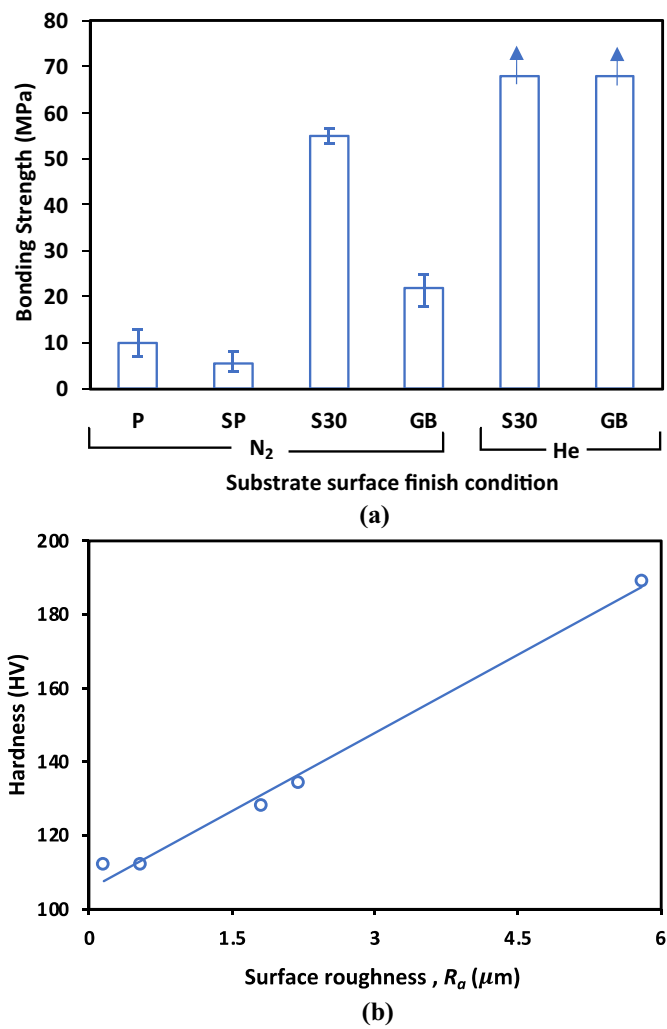


Fig. 6. (a) Bonding strength for different substrate surface finish and accelerating gases, (b) correlation of substrate hardness with surface roughness.

uncoated samples is attributed to compressive residual stress in the coatings. For Al-6061 CS deposits sprayed by He a compressive residual stress in the range of 20 MPa has been reported in [44,45]. Therefore, higher fatigue strength of coated specimens (~130 MPa) compared to that of the uncoated specimens (110 MPa) can be associated with the compressive residual stress in He-sprayed coatings. However, a lower

level of residual stress is expected for N_2 -sprayed coatings. This is indicated by the lower particle flattening ratio of the N_2 -sprayed specimens. Therefore, fatigue crack initiation and propagation are not suppressed by the low residual stress level in these specimens.

High stress fatigue performance of He-sprayed specimens was not affected significantly by the compressive residual stress (see Fig. 7b). This can be attributed to residual stress relaxation which takes place during cyclic loading [46–48]. At high stress levels, significant local plastic deformation takes place due to high stress concentration around imperfections. This results in significant rearrangement of mobile dislocations during cyclic loading, which results in releasing some portion of residual stress in the coating. Therefore, as the fatigue crack initiate from imperfections within the coating in the first few cycles, they propagate without being affected by the residual stress [46–48].

Fig. 7 also shows that the scatter in fatigue life of S30- N_2 -coated specimens is relatively high as compared to GB- N_2 -coated or He-coated samples. This is attributed to higher number of defects in the N_2 -coated specimens compared to the He-coated samples. In the GB- N_2 -coated samples, the cracks that initiate from the coating are arrested at the interface due to coating delamination, but the main cracks that result in fatigue failure initiate from the coating-substrate interface. However, in the S30- N_2 -coated specimens, the fatigue cracks that initiate from defects in the coating propagate into the substrate, leading to failure. These defects can act like cracks and can grow when a cyclic load is applied. Variation in size and location of these defects results in the scatter in fatigue life. This fact has also been reported in other defect containing materials including castings and additively manufactured specimens, in which the scatter in fatigue life has been reported up to orders of magnitude [49–55].

In order to evaluate the crack path side profile, failed specimens were sectioned along the median section and polished for metallography examination. The cross-section micrograph of the failed specimens coated with N_2 and He are shown in Fig. 10. This figure shows that in He-

Table 4

Fatigue strength at 10^7 cycles for uncoated and coated samples in different coating conditions.

	Uncoated	N_2 -S30-coated ^a	N_2 -GB-coated ^a	He-S30-coated ^b	He-GB-coated ^b
Fatigue strength (MPa)	110	99	106	133	130

^a The coating was not considered as load bearing (coating thickness was not considered for stress computation).

^b The coating was considered as load bearing (coating thickness was considered for stress computation).

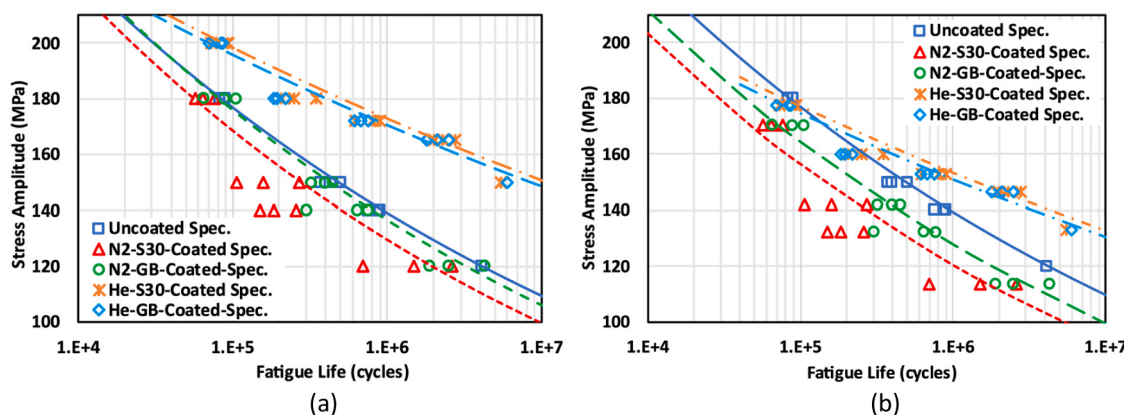


Fig. 7. SN diagrams of different groups of coated specimens in semi-log scale. The stress amplitude was computed (a) without considering the thickness of the coating, (b) with considering the coating thickness. The lines correspond to a failure probability of 90 %.

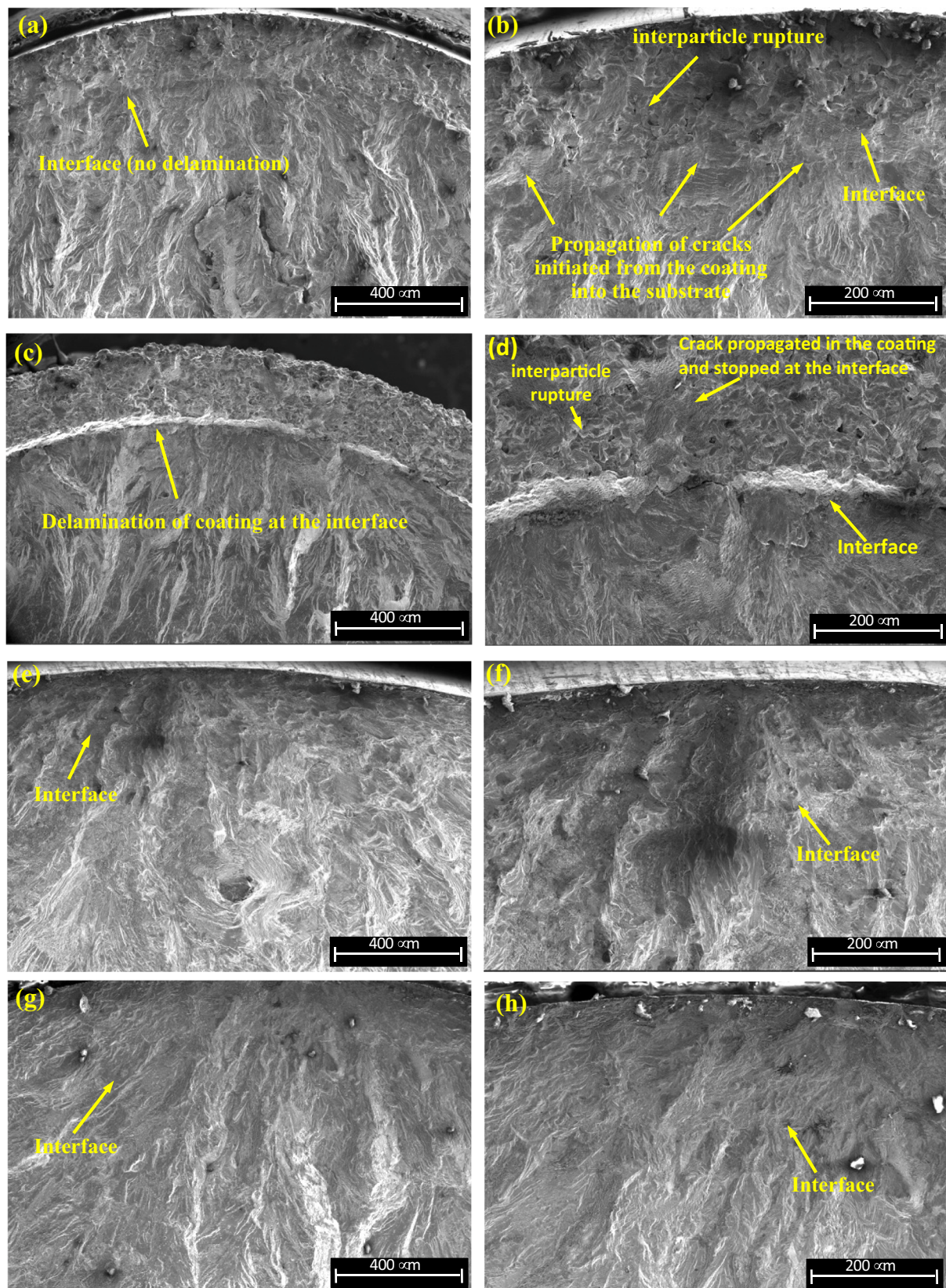


Fig. 8. SEM micrographs of fracture surfaces of, a, b) S30-N₂-coated ($\sigma_a = 140$ MPa, $N_f = 259273$ cycles), c, d) GB-N₂-coated ($\sigma_a = 140$ MPa, $N_f = 761363$ cycles), e, f) S30-He-coated ($\sigma_a = 152$ MPa, $N_f = 629186$ cycles), and g, h) GB-He-coated specimens ($\sigma_a = 152$ MPa, $N_f = 612894$ cycles).

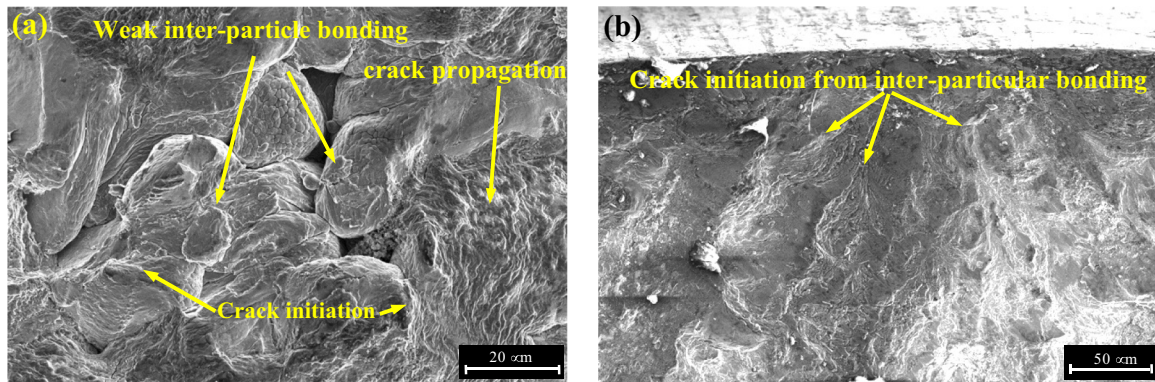


Fig. 9. Crack initiation from the coating in (a) N₂-coated specimens ($\sigma_a = 140$ MPa, $N_f = 259273$ cycles) and (b) He-coated specimens ($\sigma_a = 152$ MPa, $N_f = 612894$ cycles).

sprayed specimens, the fatigue crack propagation is mostly trans-particular, which is relatively smooth. This is due to strong bonding between the particles, resulting in crack propagation from one particle to another. However, the crack growth mechanism in the case of N₂-sprayed specimens was mix-mode failure consisting of both trans-particular and inter-particular mechanisms, indicating a partial inter-particle bonding. *Trans-particular* crack growth mechanism in He-sprayed deposits has also reported by Gavras et al. [56] and Julien et al. [57]. Gavras et al. reported a trans-particular crack growth mechanism for He-coated deposits, especially when the crack length is small.

4. Summary and conclusions

Fatigue performance of Al 6061-T6 alloy coated with Al 6061 powder under fully-reversed uniaxial loading was evaluated. Effects of

substrate surface finish and particle impact velocity on the bonding strength and fatigue performance were studied. Strength of the coating-substrate interface bonding was studied by preparing specimens with different surface finish before coating. Particle velocity was changed by using N₂ and He as accelerating gases during CS deposition. Thus, fatigue performance of coated specimens with different bonding strength and different coating qualities were evaluated and compared with uncoated samples.

A new approach, where the surface was prepared by spraying the Al 6061 particles at 30° nozzle orientation (S30), was introduced. This was shown to enhance the bonding strength between the deposit and the substrate. N₂-coated specimens experienced significant increase to their bonding strength; He-coated specimens also showed strong bonding with S30 treatment.

Evidence of stress relaxation due to partial annealing resulting from impinging hot gases was observed. Further evidence of residual stress

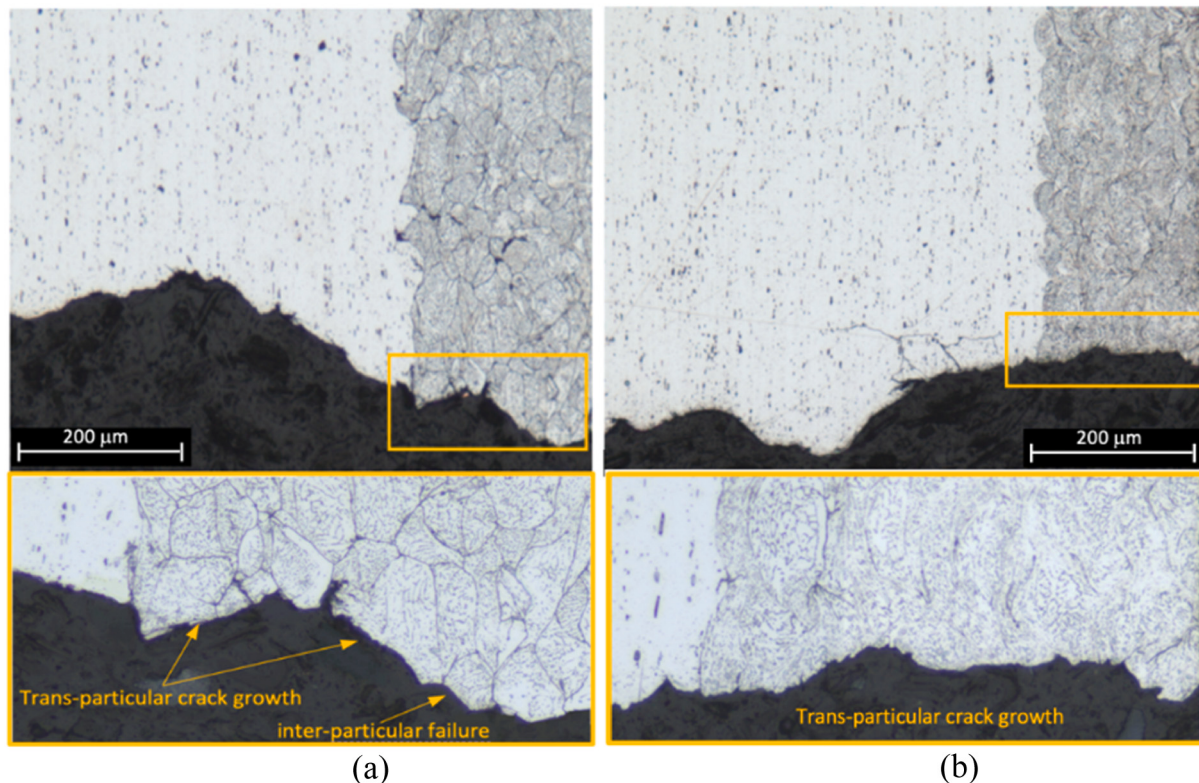


Fig. 10. Optical micrographs from the cross section of fracture surfaces of, a) S30-N₂-coated ($\sigma_a = 150$ MPa, $N_f = 272424$ cycles) and b) S30-He-coated ($\sigma_a = 160$ MPa, $N_f = 206337$ cycles) at higher magnification.

relaxation during cyclic loading, especially at high stress levels was also observed. Fatigue life of He-coated specimens were about 20% longer than the uncoated specimens at lower stress levels, but their fatigue life was comparable to or lower than the uncoated samples at high stress levels. This was attributed to residual stress relaxation during cyclic loading especially at high stress levels. The fatigue life of the N₂-coated specimens was generally lower than the uncoated specimens.

This work showed that the fatigue performance of the coatings depends on: *i*) bonding strength of the coating-substrate interface, and *ii*) the coating integrity. We found that fatigue cracks typically initiate from the imperfections in the coating and propagate toward the substrate-coating interface. If the interface bonding is sufficiently strong, the cracks can move into the substrate and could lower the fatigue life of the system. If the interface bonding is not strong, the coating delaminates, and the fatigue crack is arrested, but no improvement to the fatigue life is achieved. We also found that fatigue life of the system can be improved the most when the coating is strong and pore free.

CRediT authorship contribution statement

A. N.-A.: Study conception; Study implementation; Manuscript writing.

S. M.: Study conception; manuscript writing.

Declaration of competing interest

The authors declare that they have no known competing financial interests or personal relationships that could have appeared to influence the work reported in this paper.

Data availability

Data will be made available on request.

Acknowledgment

This work has been partially sponsored by a partnership with NAVSEA 04 and the National Center for Manufacturing Sciences under contract number 2020129-142021 to Northeastern University. The findings and opinions expressed in this paper are solely of the authors and do not necessarily represent those of the sponsors, and no official endorsement should be inferred.

References

- [1] R. Jenkins, S. Yin, B. Aldwell, M. Meyer, R. Lupoi, New insights into the in-process densification mechanism of cold spray Al coatings: low deposition efficiency induced densification, *J.Mater.Sci.Technol.* 35 (3) (2019) 427–431.
- [2] C. Chen, X. Xie, Y. Xie, X. Yan, C. Huang, S. Deng, Z. Ren, H. Liao, Metallization of polyether ether ketone (PEEK) by copper coating via cold spray, *Surf. Coat. Technol.* 342 (2018) 209–219.
- [3] R. Lima, A. Kucuk, C. Berndt, J. Karthikeyan, C.M. Kay, J. Lindemann, Deposition efficiency, mechanical properties and coating roughness in cold-sprayed titanium, *J. Mater. Sci. Lett.* 21 (2002) 1687–1689.
- [4] G. Bae, S. Kumar, S. Yoon, K. Kang, H. Na, H.J. Kim, C. Lee, Bonding features and associated mechanisms in kinetic sprayed titanium coatings, *Acta Mater.* 57 (19) (2009) 5654–5666.
- [5] H. Assadi, F. Gärtner, T. Stoltenhoff, H. Kreye, Bonding mechanism in cold gas spraying, *Acta Mater.* 51 (2003) 4379–4394.
- [6] M. Hassani-Gangaraj, D. Veysset, K.A. Nelson, C.A. Schuh, In-situ observations of single micro-particle impact bonding, *Scr. Mater.* 145 (2018) 9–13.
- [7] B. Yildirim, H. Fukunuma, T. Ando, A. Gouldstone, N.D.S. Müftü, A numerical investigation into cold spray bonding processes, *J.Tribol.* 137 (1) (2015), 011102.
- [8] W.W. Xie, A. Alizadeh-Dehkhanghani, Q. Chen, V. Champagne, X. Wang, A. Nardi, S. Kooi, S. Müftü, J. Lee, Dynamics and extreme plasticity of metallic microparticles in supersonic collisions, *Sci.Rep.* 7 (1) (2017) 1–9.
- [9] A. Moridi, S.M. Hassani-Gangaraj, M. Guagliano, M. Dao, Cold spray coating: review of material systems and future perspectives, *Surf.Eng.* 30 (6) (2014) 369–395.
- [10] Y. Li, Y. Wei, X. Luo, C. Li, N. Ma, Correlating particle impact condition with microstructure and properties of the cold-sprayed metallic deposits, *J.Mater.Sci. Technol.* 40 (2020) 185–195.
- [11] S. Yin, X. Suo, H. Liao, Z. Guo, X. Wang, Significant influence of carrier gas temperature during the cold spray process, *Surf. Eng.* 30 (6) (2014) 443–450.
- [12] S. Bagherifard, M. Guagliano, Fatigue performance of cold spray deposits: coating, repair and additive manufacturing cases, *Int. J. Fatigue* 139 (2020), 105744.
- [13] T.S. Price, P.H. Shipway, D.G. McCartney, Effect of cold spray deposition of a titanium coating on fatigue behavior of a titanium alloy, in: Proceedings of the International Thermal Spray Conference, 2006, pp. 507–512.
- [14] E. Sansoucy, G. Kim, A. Moran, B. Jodoin, Mechanical characteristics of Al-Co-Ce coatings produced by the cold spray process, *J.Thermal Spray Technol.* 16 (5–6) (2007) 651–660.
- [15] J. Barnes, V. Champagne, D. Ballard, T.J. Eden, B. Shoffner, J.K. Potter, D.E. Wolfe, Mechanical And Microstructural Effects of Cold Spray Aluminum on Al 7075 Using Kinetic Metallization And Cold Spray Processes, Lockheed Martin Aeronautical Systems, Marietta GA, 2007.
- [16] R. Ghelichi, D. MacDonald, S. Bagherifard, H. Jahed, Microstructure and fatigue behavior of cold spray coated Al5052, *Acta Mater.* 60 (19) (2012) 6555–6561.
- [17] R. Ghelichi, S. Bagherifard, D. Mac Donald, M. Brochu, H. Jahed, B. Jodoin, M. Guagliano, Fatigue strength of Al alloy cold sprayed with nanocrystalline powders, *Int. J. Fatigue* 65 (2014) 51–57.
- [18] S.B. Dayani, S.K. Shaha, R. Ghelichi, J.F. Wang, H. Jahed, The impact of AA7075 cold spray coating on the fatigue life of AZ31B cast alloy, *Surf. Coat. Technol.* 337 (2018) 150–158.
- [19] J. Yang, J. Yang, J. Xie, Q. Wang, K. Qu, Improved fatigue crack propagation performance of Q355B steel with cold-sprayed A5052 and Al coatings, *Surf. Coat. Technol.* 378 (2019), 125000.
- [20] Y. Xiong, M.X. Zhang, The effect of cold sprayed coatings on the mechanical properties of AZ91D magnesium alloys, *Surf. Coat. Technol.* 253 (2014) 89–95.
- [21] C.Y. Jeong, S. Ha, Fatig properties of Al-Si casting alloy with cold sprayed Al/SiC coating, *Int.J.Cast Met.Res.* 21 (1–4) (2008) 235–238.
- [22] S.S. Kumar, G. Bae, C. Lee, Influence of substrate roughness on bonding mechanism in cold spray, *Surf. Coat. Technol.* 304 (2016) 592–605.
- [23] G. Bae, S. Kumar, S. Yoon, K. Kang, H. Na, H.J. Kim, C. Lee, Bonding features and associated mechanisms in kinetic sprayed titanium coatings, *Acta Mater.* 57 (19) (2009) 5654–5666.
- [24] T. Hussain, D.G. McCartney, P.H. Shipway, D. Zhang, Bonding mechanisms in cold spraying: the contributions of metallurgical and mechanical components, *J. Therm. Spray Technol.* 18 (3) (2009) 364–379.
- [25] T. Marrocco, D.G. McCartney, P.H. Shipway, A.J. Sturgeon, Production of titanium deposits by cold-gas dynamic spray: numerical modeling and experimental characterization, *J. Therm. Spray Technol.* 15 (2) (2006) 263–272.
- [26] J. Wu, J. Yang, H. Fang, S. Yoon, C. Lee, The bond strength of Al-Si coating on mild steel by kinetic spraying deposition, *Appl. Surf. Sci.* 252 (22) (2006) 7809–7814.
- [27] C.W. Zieman, M.M. Sharma, B.D. Bouffard, T. Nissley, T.J. Eden, Effect of substrate surface roughening and cold spray coating on the fatigue life of AA2024 specimens, *Mater. Des.* 54 (2014) 212–221.
- [28] A. Moridi, S.M. Hassani-Gangaraj, S. Vezzù, L. Trško, M. Guagliano, Fatigue behavior of cold spray coatings: the effect of conventional and severe shot peening as pre-/post-treatment, *Surf. Coat. Technol.* 283 (2015) 247–254.
- [29] D. Jafarloo, G. Ferguson, K.L. Tsakopoulos, A.C. Chuang, A. Nardi, D. Cote, I. Grosse, Structural integrity of additively manufactured stainless steel with cold sprayed barrier coating under combined cyclic loading, *Addit.Manuf.* 35 (2020), 101338.
- [30] J. Bi, Z. Loke, C. Lim, K. Teng, P. Koh, Mechanical properties of cold sprayed aluminium 2024 and 7075 coatings for repairs, *Aerospace* 9 (2) (2022) 65.
- [31] ASM Handbook vol. 2, ASM International, Materials Park, OH, 1990.
- [32] W.C. Evans, X. Dan, A. Houshmand, S. Müftü, T. Ando, Microstructural characterization of aluminum 6061 splats cold spray deposited on aluminum 6061-T6 substrate, *Metall. Mater. Trans. A* 50 (8) (2019) 3937–3948.
- [33] J. Pattison, S. Celotto, A. Khan, W. O'Neill, Standoff distance and bow shock phenomena in the Cold Spray process, *Surf.Coat.Technol.* 202 (8) (2008) 1443–1454.
- [34] X.T. Luo, Y. Li, C.X. Li, G.J. Yang, C.J. Li, Effect of spray conditions on deposition behavior and microstructure of cold sprayed Ni coatings sprayed with a porous electrolytic Ni powder, *Surf. Coat. Technol.* 289 (2016) 85–93.
- [35] D.L. Gilmore, R.C. Dykhuijen, R.A. Neiser, T.J. Roemer, M.F. Smith, Particle velocity and deposition efficiency in the cold spray process, *J. Therm. Spray Technol.* 8 (4) (1999) 576–582.
- [36] C.J. Li, W.Y. Li, Y.Y. Wang, H. Fukunuma, Effect of spray angle on deposition characteristics in cold spraying, *Therm. Spray* (2003) 91–96.
- [37] ASTM C633 – 13, Standard Test Method for Adhesion Or Cohesion Strength of Thermal Spray Coatings, 2017.
- [38] ASTM E466 – 21, Standard Practice for Conducting Force Controlled Constant Amplitude Axial Fatigue Tests of Metallic Materials, 2021.
- [39] ASTM E739 – 10, Standard Practice for Statistical Analysis of Linear Or Linearized Stress-life, 2015.
- [40] A.A. Tamiyu, C.A. Schuh, Particle flattening during cold spray: mechanistic regimes revealed by single particle impact tests, *Surf. Coat. Technol.* 403 (2020), 126386.
- [41] E.E. Calla, D. McCartney, P. Shipway, Deposition of copper by cold gas dynamic spraying: an investigation of dependence of microstructure and properties of the deposits on the spraying conditions, in: Advances in Technology And Application: Proceedings of the International Thermal Spray Conference, 2004, pp. 20–30.
- [42] R. Huang, H. Fukunuma, Study of the influence of particle velocity on adhesive strength of cold spray deposits, *J. Therm. Spray Technol.* 21 (3–4) (2012) 541–549.
- [43] A.A.W.Y. Tan, W. Sun, A. Bhowmik, J.Y. Lek, X. Song, W. Zhai, H. Zheng, F. Li, I. Marinescu, Z. Dong, E. Liu, Effect of substrate surface roughness on

- microstructure and mechanical properties of cold-sprayed Ti6Al4V coatings on Ti6Al4V substrates, *J. Therm. Spray Technol.* 28 (8) (2019) 1959–1973.
- [44] M.R. Rokni, C.A. Widener, O.C. Ozdemir, G.A. Crawford, Microstructure and mechanical properties of cold sprayed 6061 Al in as-sprayed and heat-treated condition, *Surf. Coat. Technol.* 309 (2017) 641–650.
- [45] M. Saleh, V. Luzin, K. Spencer, Analysis of the residual stress and bonding mechanism in the cold spray technique using experimental and numerical methods, *Surf. Coat. Technol.* 252 (2014) 15–28.
- [46] J.J.C. Kim, S.K. Cheong, H. Noguchi, Residual stress relaxation and low-and high-cycle fatigue behavior of shot-peened medium-carbon steel, *Int. J. Fatigue* 56 (2013) 114–122.
- [47] D. Rao, D. Wang, L. Chen, C. Ni, The effectiveness evaluation of 314L stainless steel vibratory stress relief by dynamic stress, *Int. J. Fatigue* 29 (1) (2007) 192–196.
- [48] W.Z. Zhuang, G.R. Halford, Investigation of residual stress relaxation under cyclic load, *Int. J. Fatigue* 23 (2001) 31–37.
- [49] S. Romano, A. Brückner-Foit, A. Brandão, J. Gumpinger, T. Ghidini, S. Beretta, Fatigue properties of AlSi10Mg obtained by additive manufacturing: defect-based modelling and prediction of fatigue strength, *Eng. Fract. Mech.* 187 (2018) 165–189.
- [50] M. Shamir, A.K. Syed, V. Janik, R. Biswal, X. Zhang, The role of microstructure and local crystallographic orientation near porosity defects on the high cycle fatigue life of an additive manufactured Ti-6Al-4V, *Mater. Charact.* 169 (2020), 110576.
- [51] Y.W. Luo, B. Zhang, C.P. Li, G.F. Chen, G.P. Zhang, Detecting void-induced scatter of fatigue life of selective laser melting-fabricated Inconel 718 using miniature specimens, *Mater. Res. Express* 6 (4) (2019), 046549.
- [52] A. Nourian-Avval, A. Fatemi, Fatigue life prediction of cast aluminum alloy based on porosity characteristics, *Theor. Appl. Fract. Mech.* 109 (2020), 102774.
- [53] A. Nourian-Avval, A. Fatemi, Fatigue design with high pressure die cast aluminum including the effects of defects, section size, stress gradient, and mean stress, *Mater. Today Commun.* 25 (2020), 101567.
- [54] A. Nourian-Avval, A. Fatemi, Fatigue performance and life prediction of cast aluminum under axial, torsion, and multiaxial loadings, *Theor. Appl. Fract. Mech.* 111 (2021), 102842.
- [55] A.A. Nourian-Avval, A. Fatemi, Variable amplitude fatigue behavior and modeling of cast aluminum, *Fatigue Fract. Eng. Mater. Struct.* 44 (6) (2021) 1611–1621.
- [56] A.G. Gavras, D.A. Lados, V.K. Champagne, R.J. Warren, Effects of processing on microstructure evolution and fatigue crack growth mechanisms in cold-spray 6061 aluminum alloy, *Int. J. Fatigue* 110 (2018) 49–62.
- [57] S. Julien, A. Nourian-Avval, W. Liang, T. Schwartz, O. Ozdemir, S. Müftü, Bulk fracture anisotropy in cold-sprayed Al 6061 deposits, *Eng. Fract. Mech.* 108301 (2022).